Catalysis Today 432 (2024) 114620

Contents lists available at ScienceDirect

Catalysis Today

journal homepage: www.elsevier.com/locate/cattod

Acid treatment enhances the methane combustion activity of $LaFeO_3$ perovskite catalyst

Xiaochao Wu [a,b,*], Mengyang Li [a], Ahed Abouserie [a,b], Anne Frommelius [a], Gianluca Dalfollo [a], Thorsten Ohlerth [a], Ulrich Simon [a,b]

[a] *Institute of Inorganic Chemistry, RWTH Aachen University, Landoltweg 1a, Aachen 52074, Germany*
[b] *Center for Automotive Catalytic Systems Aachen, RWTH Aachen University, Schinkelstraße 8, Aachen 52062, Germany*

ARTICLE INFO

Keywords:
Methane combustion
Perovskite oxides
$LaFeO_3$
Surface modification
Acid treatment

ABSTRACT

The catalytic combustion of methane has gained much attention as a sustainable technology, due to concerns about the environmental impact of unburnt methane emissions from the natural gas vehicles. Researchers have explored alternatives to precious metal catalysts for methane combustion, with a focus on perovskite oxides known for their excellent activity and sintering-resistance capacity. In this study, $LaFeO_3$ perovskite material was synthesized and subsequently subjected to a nitric acid etching treatment to modify its surface. It was found that the acid preferentially dissolved La cations from $LaFeO_3$ surface while the perovskite phase was unchanged, as a consequence, the etched $LaFeO_3$ shows improvement in methane combustion activity. The best performance was achieved in the sample with one-hour surface etched treatment, which suggests that the appropriate surface reconstruction induced by acid treatment promotes the formation of more active Fe sites on the surface and reduces the energic barriers of methane activation. This work presents a straightforward and effective approach to tailor the exposed surface properties of perovskites, thereby enhancing their activity in hydrocarbon combustion reactions.

1. Introduction

Methane (CH_4), as the main component of natural gas, has become more common as an industrial fuel across the world and has led to an increase in natural-gas-powered land vehicles and ships. However, the presence of unburnt CH_4 in the exhaust affects the fuel economy, as its huge greenhouse effect, which exceeds that of CO_2 by a factor of 25, requires efficient catalytic combustion as well as effective exhaust gas aftertreatment strategies to minimize its emission [1–3]. Therefore, from the energy or environmental perspective, the reasonable and effective utilization of CH_4 is an imperative problem that needs to be solved. One of the most promising solutions for the use of natural gas appears to be the complete combustion of CH_4 in the presence of catalysts [4–6], which has been applied in many areas. Catalytic combustion could lower light-off temperatures, improve CH_4 utilization efficiency, and reduce emissions. Consequently, the catalytic combustion of CH_4 as a clean technology has received increasing research attention and considerable efforts are being performed towards optimized catalyst systems [7–9].

Among the CH_4 combustion catalysts, perovskite oxides exhibit significant potential in the realm of heterogeneous catalysis [10,11]. This is primarily attributed to the inherent nature of transition metal contributions, which frequently exist in multiple valence states [12]. This characteristic enables the seamless interplay of redox cycles between higher and lower oxidation states. Concurrently, lattice oxygen can be liberated and subsequently regenerated, further enhancing their catalytic capabilities [13]. $LaFeO_3$, belonging to the typical perovskite oxide, exhibits quite improved resistance against high temperatures under the fluctuating catalytic reaction conditions of automobile exhaust gases [14].

As the surface characteristics of catalysts are critical for the heterogeneous reaction, controlling the regulation of the surface is an efficient technique to improve their catalytic activity [15–17]. The results of density functional and molecular dynamics studies have revealed that the B-site cation, rather than the A-site cation, controls the catalytic activity or adsorption sites of perovskites [18,19]. The A-site cation is located at the edge of the structure and is used to stabilize the structure and has less influence on the catalytic activity. However, natural

---

[*] Corresponding author at: Institute of Inorganic Chemistry, RWTH Aachen University, Landoltweg 1a, Aachen 52074, Germany.
E-mail address: xiaochao.wu@ac.rwth-aachen.de (X. Wu).

https://doi.org/10.1016/j.cattod.2024.114620
Received 20 December 2023; Received in revised form 21 February 2024; Accepted 29 February 2024

perovskite surfaces are predominantly A-site rich [20], which may hinder to unfold of their full catalytic potential. A straightforward method to produce more B-site (rich) terminated perovskite surfaces and associated catalytic property studies are essential to solve the above issues. For ABO_3 perovskites, single A-O bonds are usually longer than B-O bonds and have higher surface energy [21], which theoretically offers the possibility of selectively removing A-site cations from the perovskite backbone. Huang et al. [22] firstly reported a wet etching treatment of Mn-based perovskite catalysts to change the catalytic activity for CO oxidation by dipping with dilute HNO_3 solution, which provides new possibilities for selective removal of A-site cations. Yang et al. [23] demonstrated a facile surface modification strategy by immersing $La_{0.8}Sr_{0.2}CoO_3$ perovskite in an oxalic acid solution, introducing both oxygen vacancies and Co^{n+} Lewis acid sites, which resulted in favorable CH_4 oxidation. Because of their enhanced resistance against high temperature in the variable catalytic reaction environments of automobile exhaust gases [24], $LaFeO_3$ perovskites show promising potentials for catalytic oxidation reactions. Nevertheless, their intrinsic reactivity is not the most among the perovskite oxides, which deserves to be further modified.

In this study, we employed a sol-gel method to synthesize $LaFeO_3$ perovskite and subsequently subjected it to a surface modification process by using nitric acid etching treatment. The physical and chemical properties were characterized, and the results show that acid preferentially dissolved La cations from the $LaFeO_3$ surface, while the perovskite phase was unchanged. The selective dissolution altered the ratio of La/Fe, particularly on the surface, which had a discernible impact on the catalytic reactivity. CH_4 combustion was employed as the probe reaction to study the catalytic activity, and the relationship of etching treatment time and the CH_4 conversion temperature was investigated. This work presents a straightforward and effective approach to tailor the exposed surface properties of perovskites, thereby enhancing their activity in hydrocarbon combustion reactions.

2. Experiment section

2.1. Materials

The chemical reagents were purchased from Sigma-Aldrich Company (Germany). All chemicals were analytically pure and ready for use without further purification. $La(NO_3)_3 \cdot 6H_2O$ (0.01 mol, 4.33 g), $Fe(NO_3)_3 \cdot 9H_2O$ (0.01 mol, 4.04 g), and citric acid (0.015 mol, 2.88 g) were added to 100 mL of ultrapure water and stirred continuously until fully dissolved. Water was evaporated from the mixed solution at 80 °C for around 4 h, to obtain a viscous gel. The gel was moved to the oven overnight at 140 °C. The resulting glassy material was grounded and calcined in muffle oven to 300 °C at 60 °C h^{-1} and held for 2 h, then up to 700 °C at 115 °C h^{-1} and held for 5 h. The prepared catalyst was noted as LFO. 0.5 g of above prepared LFO was suspended in 40 mL of 0.5 M nitric acid for x h (x = 0.5, 1, 2) at room temperature. The suspension was centrifuged and washed several times with ultrapure water and ethanol to remove the residual nitric acid. The samples were dried overnight at 100 °C to obtain the etched perovskite catalysts, labeled as LFO-Hx.

2.2. Characterization

Powder X-ray diffraction (pXRD) was performed using a STOE STADIP MP X-ray powder diffractometer (STOE and Cie GmbH, Darmstadt, Germany). The X-ray generator was equipped with a molybdenum tube operating at 50 kV and 40 mA, irradiating the sample with monochromatic Mo $K_{\alpha1}$ (λ= 0.709300 Å). XRD patterns were recorded at room temperature for 240 min over a 2θ range of 2–80° with a step size of 0.195°. Scanning electron microscopy (SEM) was performed on an FE-SEM LEO/Zeiss Supra 35 VP equipped with an Oxford Instruments INCA x-act detector to determine elemental distribution mapping using energy dispersive X-ray (EDX) spectroscopy. Bright-field transmission electron microscopy (TEM) and scanning transmission electron microscopy (STEM) images were recorded with a ZEISS LIBRA 200 FE microscope operating at 200 kV. X-ray fluorescence (XRF) spectroscopy was performed on the powder and the solution with a micro-X-ray fluorescence spectrometer (EAGLE μ-Probe II, (Oxford Instruments, Abingdon, GB-OXF)) with a 300 μm capillary and operated at 40 kV using a Rh target. Brunauer–Emmett–Teller (BET) surface area was obtained with a Micromeritics ASAP 2060 Instrument (Micromeritics) by measuring the nitrogen physisorption at a temperature of 77 K after degassing (0.4 kPa total pressure at 523 K for 4 h). H_2-temperature programmed reduction (H_2-TPR) was carried out on an Autosorb iQ (Quantachrome Instruments) with a TCD detector. The materials were heated to 400 °C (10 °C/min) under N_2 gas flow for one hour as a pretreatment process. After it cooled down to room temperature, the gas was switched to 10 % H_2 in Ar. Temperature was increased to 800 °C with a rate of 10 °C/min and the signal from the TCD was recorded against the temperature. X-ray photoelectron spectroscopy (XPS, PHI5000 VersaProbe spectrometer equipped with an Al K_α X-ray source). The binding energies were calibrated to the adventitious C 1s peak at 284.8 eV, and data were fitted by the public software package XPSPEAK. *In-situ* diffuse reflectance infrared Fourier transform (DRIFTS), the LFO-H1 powder (approx. 50 mg) was placed inside a high-temperature reaction chamber (HVC−DRP, Harrick Scientific Products, Inc.). Infrared spectroscopy in Kubelka-munk mode was applied using an FT-IR VERTEX 70 device (Bruker) and a Harrick Praying Mantis mirror system. The samples were heated to 300 °C and held at that temperature for 1 h in a N_2 stream (with a flow rate of 100 mL min^{-1}) for the pretreatment. After that, the chamber with the sample was heated up and kept at 550 °C. The spectrum of N_2 was recorded as background and subtracted from the spectra collected afterward. Then, a flow of 1 % CH_4, 10 % O_2 and balance N_2 (total, 100 mL min^{-1}) was fed onto the catalyst surface, and the spectra were collected by repeatable measurement mode for 30 minutes.

2.3. Catalyst activity measurements

200 mg of prepared samples were loaded into a cylindrical glass tube reactor with a diameter of 1 cm and fixed with quartz wool. For pretreatment, the tube reactor with the catalyst was heated in N_2 up to 300 °C at a ramping rate of 7.5 °C min^{-1} in a vertical tube furnace (RS232, HTM Reetz GmbH) and then held at constant temperature for 1 h. Then the gas feed was changed to a mixture of 200 mL min^{-1} $CH_4/O_2/N_2$ to study the CH_4 combustion. The gas flow composition was:

$\Phi_{CH4} = 1$ Vol%

$\varphi_{O2} = 10$ Vol%

$\varphi_{N2} = 89$ Vol%

CH_4 combustion light-off curves were collected in a temperature range of 300–700 °C with a temperature ramp rate of 10 °C min^{-1} and maintained at a constant temperature of one hour per 50 °C. The outlet gas composition was analyzed by an FTIR gas analyzer (Model 2030, MKS INSTRUMENTS). The standard deviation of CH_4 conversions, obtained by averaging the CH_4 conversion data for each individual temperature, is consistently below 0.04 for all catalysts. CH_4 conversion was calculated using Eq. (1).

$$CH_4 \quad conversion : X = \frac{(C_{CH_{4,in}} \quad - C_{CH_{4,out}})}{C_{CH_{4,in}}} \times 100\% \tag{1}$$

Where X is the CH_4 conversion at specific temperature and $C_{CH_{4,in}}$ and $C_{CH_{4,out}}$ are the reactor inlet and outlet CH_4 concentrations, respectively.

3. Results and discussion

Based on the etching treatment time (0.5, 1, 2 h), the obtained samples are named as LFO-Hx (x = 0.5, 1, 2). Fig. 1 shows the powder X-

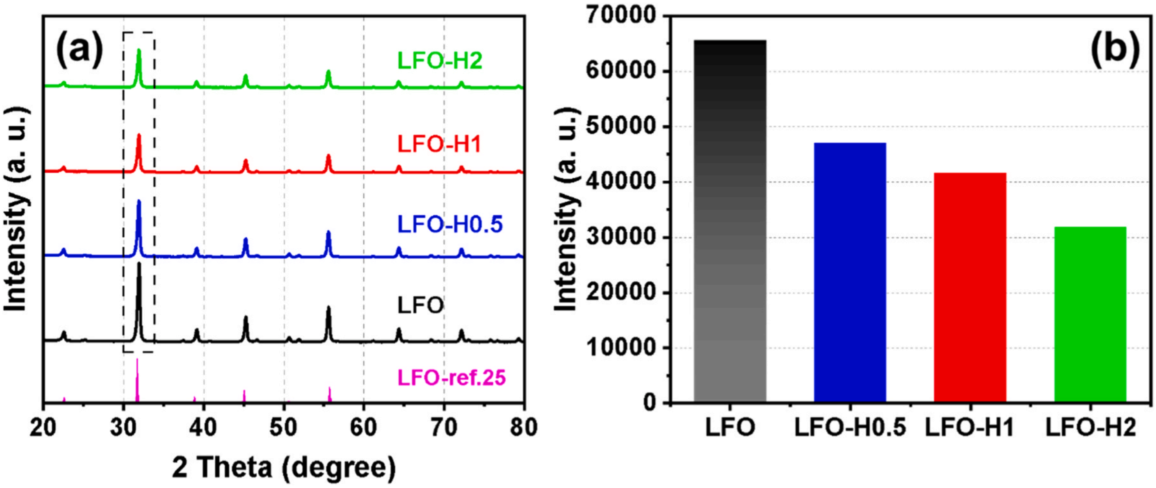

Fig. 1. (a) pXRD patterns of pristine LFO and LFO-Hx (x = 0.5, 1, 2) materials, (b) the intensities of (121) diffraction peaks.

ray diffraction (pXRD) patterns of the pristine perovskite $LaFeO_3$ (LFO) and LFO-Hx samples. The pXRD diffraction peak of the pristine LFO is in agreement with the standard $LaFeO_3$ (ICSD_258500) [25], indicating an orthorhombic perovskite structure with *Pnma* space group. Upon analyzing the changes of pXRD patterns after acid etching, it is evident that no secondary phases emerge and the original perovskite structure is maintained after etching, which indicates that the acid etching did not compromise the overall structure of LFO. A careful inspection of the (121) peaks shown in Figure S1 reveals that there are no discernible shifts in the diffraction peaks after the acid etching, indicating that no lattice expansion or crystal structure change occurred during the acid treatment [26]. Furthermore, it is worth noting that the intensities of the (121) diffraction peaks (Fig. 1b) reveal a continuous decrease as the acid treatment time is increased, proving that the crystallinity of the samples decreased.

Scanning electron microscopy (SEM) was used to reveal the morphological evolution after nitric acid treatment. As displayed in Fig. 2a–d, the pristine LFO displays a microstructure of nanoparticle stacks with primary particle sizes in the several ten nanometers range, while the nitric acid etching treatment did not significantly change the size and morphology. These samples were further characterized using transmission electron microscopy (TEM) and scanning transmission electron microscopy (STEM). As shown in Figure S2, bright field TEM images exhibit no significant distinction, the slight difference in contrast along the particle edges could be attributed to the different electron densities on the particle surface as a result of the acid etching effect. From the STEM images in Fig. 2e–h, it is obvious that the meso-pores are formed in the LFO-Hx samples, indicating a noticeable increase in the surface porosity. Hence, the metal leaching leads to a significant enhancement in surface roughness as the duration of acid etching treatment increases, implying potential surface restructuring. This is further clarified by the pore size distribution analysis in Figure S3, where the pore volume around the 7 nm region is substantially increased, especially from LFO to LFO-H2. At the same time, the porosity in a higher region, around 30 nm, is decreased. This indicates that the acid leaching can selectively enhance the porosity in smaller domains, which is consistent with the overall increase of surface roughness. The augmentation of surface roughness serves to amplify the contact area

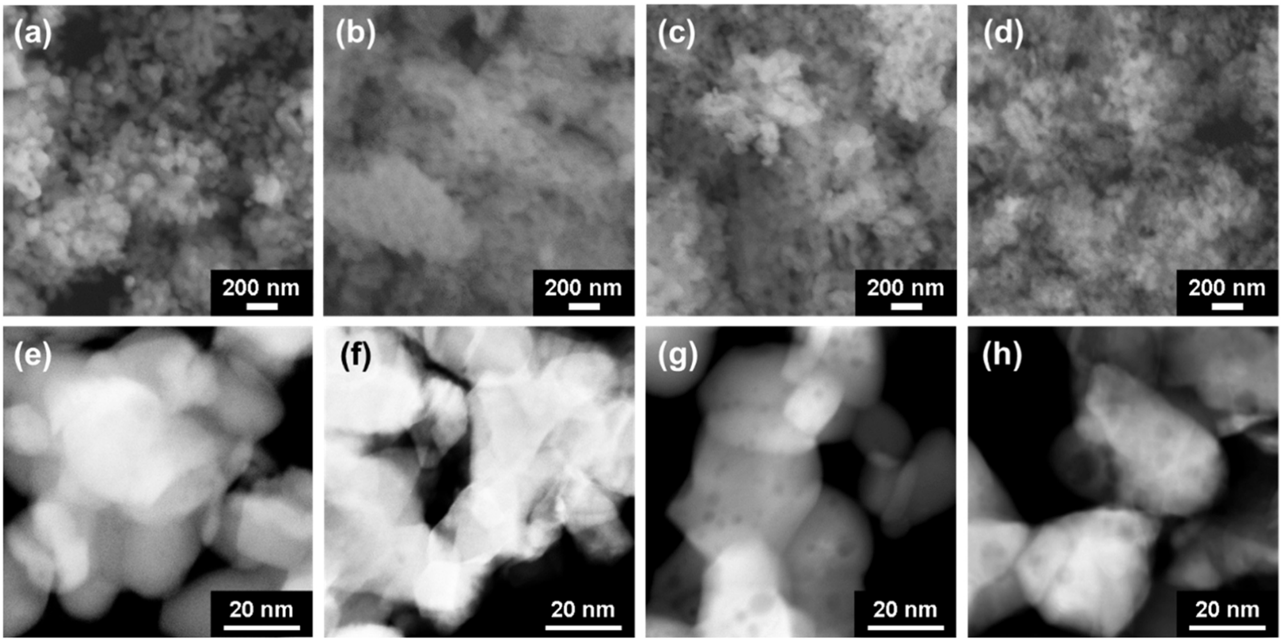

Fig. 2. SEM and STEM images of (a, e) pristine LFO and (b-d, f-h) LFO-Hx (x = 0.5, 1, 2) materials.

between the reactive species and the catalyst surface, consequently facilitating the catalytic reaction [27]. To determine the exact specific surface area of the samples, BET surface area was tested by using nitrogen (N_2) physisorption. Figure S4 displays the N_2 adsorption-desorption isotherms of pristine LFO and LFO-Hx samples, with all curves exhibiting a similar IV-type isotherm. A noticeable hysteresis loop within the relative pressure range of 0.9–1.0 can be observed, which is attributed to the inter particle pores [27]. After the acid treatment, the hysteresis loops become more pronounced, and it shows higher volume of N_2 adsorbed at P/P_0 close to 1, suggesting an enhancement in the mesoporosity of LFO-Hx. In Table 1, the BET surface area values of LFO, LFO-H0.5, LFO-H1, and LFO-H2 are 11.1, 16.0, 15.2, and 21.2 m^2 g^{-1}, respectively. Obviously, the acid etched perovskite LFO-Hx samples have a higher BET surface area, which may provide more surface catalytic active sites, thus promoting the catalytic activity of LFO-Hx samples. Table 1 also presents the metal contents of prepared samples, as determined through X-ray fluorescence (XRF) spectroscopy. After the normalization of Fe content, the La/Fe ratio decreased with a longer acid treatment time, suggesting that La cations dissolved at a higher rate than Fe cations in the nitric acid solutions, aligning with the previous studies [10,18]. In addition, to address the potential washing effect, the pristine LFO sample underwent a washing procedure with ultrapure water identical to that applied to LFO-Hx samples. XRF result (see Table S1) reveals a tiny change in the La/Fe ratio between pristine LFO and washed LFO, suggesting a negligible impact of washing on the pristine LFO.

To determine the metal ions content in treated nitric acid solution, a color reaction was initiated by mixing these solutions with NaOH, as depicted in Figure S5. Up to 1-h etching, neither Fe or La was undetectable. Notably, the LFO-H2 sample exhibited a brown-yellow color, attributed to the presence of Fe^{3+}, whereas La^{3+} being colorless, remained imperceptible in this experiment. The color reaction serves a qualitative propose to identify Fe^{3+} ions. To qualitatively assess the concentrations of La and Fe treated in the nitric acid solutions, XRD measurements were applied in triplicate, and the results of metal ions content are displayed in Table S2. With the extension of the treatment time, the La/Fe ratio in nitric acid solution rose. However, the correlation between Fe content and treated time is not linear, instead, the Fe dissolution rate gradually decreased as the acid treatment time increased. The La content was slightly higher than Fe, falling within the same range, which can be attributed to its higher solubility in nitric acid solution. The individual La-O bonds are typically longer and have a higher surface energy in comparison to Fe-O bonds, making it possible to selectively remove La [18].

The elemental compositions and surface chemical states of pristine LFO and LFO-H1 were analyzed by using X-ray photoelectron spectroscopy (XPS). In the survey spectra (see Figure S6), the characteristic peaks of La and Fe elements are observed for both samples, while no evidence for the presence of nitrogen was found for LFO-H1. The results of the La and Fe composition are summarized in Table 2. After 1-h acid treatment, there was a marked increase in Fe content, demonstrating a selective removal of La cations by nitric acid. As shown in Fe2p spectra in Fig. 3a, the peaks located at binding energies of 710.2 and 723.5 eV are attributed to $Fe2p_{3/2}$ and $Fe2p_{1/2}$, respectively [28]. Moreover, it is noteworthy that Fe2p peaks shift to higher binding energies, signifying that the surface electron density decreased and the valence of the surface Fe increased [24]. Following a peak fitting, the Fe2p spectrum is deconvoluted into three components: Fe^{2+}, Fe^{3+}, and Fe^{4+}, where the peaks at 710.5 and 723.1 eV belong to Fe^{2+}, while the peaks at 711.8 and 724.8 eV belong to Fe^{3+}. Fe^{4+} peaks are enhanced after one hour of nitric acid treatment at 714.0 and 727.1 eV. Additionally, the unobvious peaks at around 720 eV are assigned to the satellite peaks of Fe2p [29]. The presence of higher oxidation states of Fe, particularly the uncommon Fe^{4+}, could promote the CH_4 combustion activity [30]. In addition, upon integrating the peak areas of Fe in various oxidation states, the compositions of Fe with different oxidation states are summarized in the Table 2: the content of Fe^{2+} decreased by nearly 20 %, while the content of Fe in the higher oxidation states (Fe^{3+} and Fe^{4+}) increased significantly, primarily due to the strong oxidation nature of nitric acid. In the La3d XPS spectrum of pristine LFO (Fig. 3b), four component peaks were identified at the binding energies of 834.9, 838.9, 851.6 and 855.6 eV, corresponding to $La3d_{5/2}$, $La3d_{3/2}$, and their satellite peaks, respectively [31]. Notably, the peaks show a slight shift towards higher binding energies from LFO to LFO-H1. These spectra indicate the La assigned to La^{3+} valence state in both LFO and LFO-H1 samples, while the O in LFO-H1 exhibits a more negative state, thereby altering the chemical environment of La [24]. Due to the electron transfer from the O2p valence band to an empty La 4 f orbit, the change of the O chemical state also corresponds to the shake-up state of La3d [32].

Table 1
Metal content and BET surface areas of the prepared samples, normalized by La.

Sample name	XRF results			BET surface area (m^2 g^{-1})
	La	Fe	La/Fe ratio	
LFO	0.519	0.490	1.05	11.1
LFO-H0.5	0.510	0.502	1.01	16.0
LFO-H1	0.510	0.503	1.01	15.2
LFO-H2	0.511	0.511	1.00	21.2

Table 2
Surface multivalent Fe compositions of LFO and LFO-H1.

Sample name	XPS survey		XPS Fe2p		
	La	Fe	Fe^{2+}	Fe^{3+}	Fe^{4+}
LFO	59.1 %	40.9 %	44.1 %	34.9 %	21.0 %
LFO-H1	52.3 %	47.7 %	24.7 %	49.2 %	26.1 %

H_2-TPR experiments were applied to investigate the reducibility of pristine LFO and the LFO-Hx catalysts. As La^{3+} can hardly be reduced below 1000 °C, the analysis of H_2-TPR results focused on the reduction of Fe ions [33]. As displayed in Figure S7, all materials exhibit reduction peaks in the range of 250–600 °C, which can be delineated into two regions. At lower temperature range, the first series peaks located between 260 and 350 °C is attributed to the reduction of Fe^{4+} to Fe^{3+}. The second series peaks located at 400–550 °C is corresponded to the reduction of Fe^{3+} to Fe^{2+} and the surface chemisorbed bulk oxygen [33–35]. The first and largest reduction peaks shifted towards lower temperatures, suggesting that the acid treatment led to enhanced reducibility and can thereby improve the catalytic activity [36].

The catalytic activity of the pristine and the acid-etched samples was evaluated as a function of temperature in a gas flow containing 1 % CH_4 and 10 % O_2. A gas analyzer (GA) was applied to detect the gas compositions under CH_4 combustion reaction. As shown in Fig. 4, the catalytic activity improves with nitric acid treatment compared with the pristine LFO catalyst. For the conversion of CH_4 into CO_2, $T_{50\ \%}$ (the light-off temperature) for sample LFO-H0.5, LFO-H1, LFO-H2 are 550, 537 and 562 °C, and $T_{90\ \%}$ (the temperature of the conversion 90 %) are 600, 593 and 617 °C, respectively. The acid treatment led to the partial dissolution of La ions and thus to the modification of the top-monolayer surface composition by creating more Fe- termination. This alteration influences both the reactivity of the surface and the density of surface intermediates [10]. As the surface Fe-termination and La-Fe termination offer lower energetic barriers for CH_4 activation, the acid treated LFO-Hx samples exhibit enhanced catalytic activities. The best condition in our set of experiments is one hour of treatment, which lowers $T_{50\ \%}$ by 63 °C in comparison to LFO. However, when the treatment time was extended to two hours, the catalytic activity declines again. We conclude that with increasing treatment duration the Fe cations start to dissolve in nitric acid as well. Consequently, this dissolution results in a decrease in activity. Furthermore, the catalytic activities of pristine LFO and washed LFO were compared in Figure S8. The minimal difference indicates the

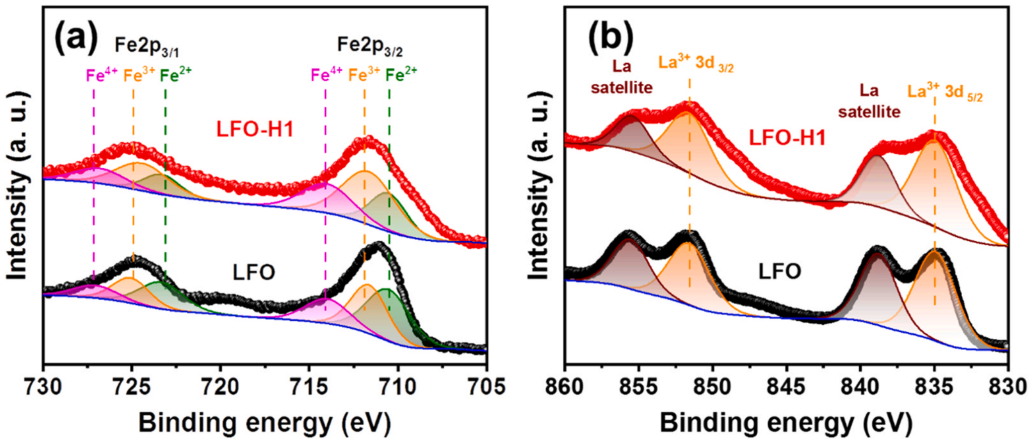

Fig. 3. XPS spectra for pristine LFO and LFO-H1: (a) Fe2p spectra, (b) La3d spectra.

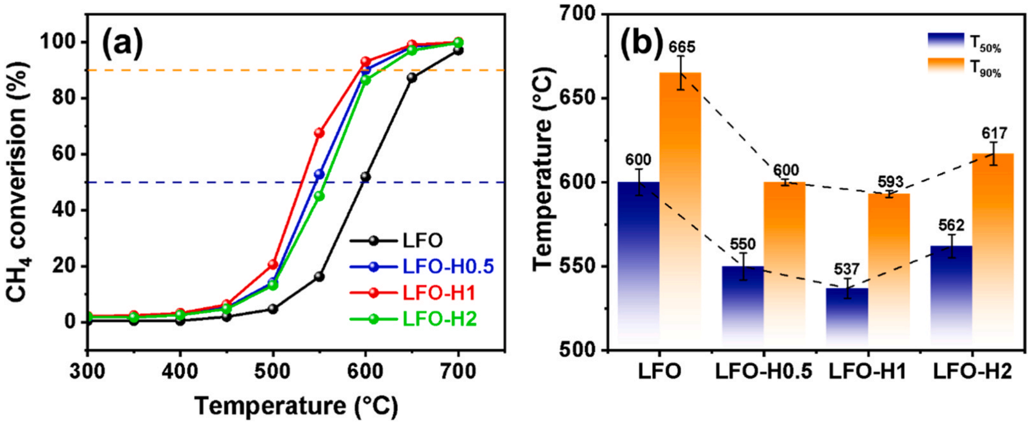

Fig. 4. Catalytic activity of CH_4 combustion over pristine LFO and LFO-Hx after acid treatment.

tiny impact of washing on the pristine LFO catalyst.

To gain deeper insights into the catalytic mechanism and reaction pathway of CH_4 combustion reaction over the acid treated $LaFeO_3$, DRIFTS experiments were performed. Fig. 5 shows the *in-situ* temperature-programmed DRIFTS results of LFO-H1 under the same gas flow conditions with catalytic activity evaluations from 350 °C to 550 °C. In the wavenumber range of 3500–2000 cm^{-1}, the distinct bands at 3265 and 3016 cm^{-1} emerge as the temperature increases, which correspond to the stretching vibration of O-H compounds from hydroxyls bond and ν_{as} C-H of gaseous CH_4, respectively [37,38]. Gradually, the absorption bands at 2359 and 2312 cm^{-1} appear at higher temperatures, which are attributed to the C═O stretching mode in gaseous CO_2 [39]. According to Cao et al., the detection of these bands indicates that methane combustion took place with lattice oxygen of $LaFeO_3$ [38]. In the low wavenumber range shown in Fig. 5b, more adsorption bands can be observed, which help to understand the catalytic mechanism. Specifically, the sharp band at 1305 cm^{-1} corresponds to δ C-H vibrations of gaseous CH_4, which supports the exitance of

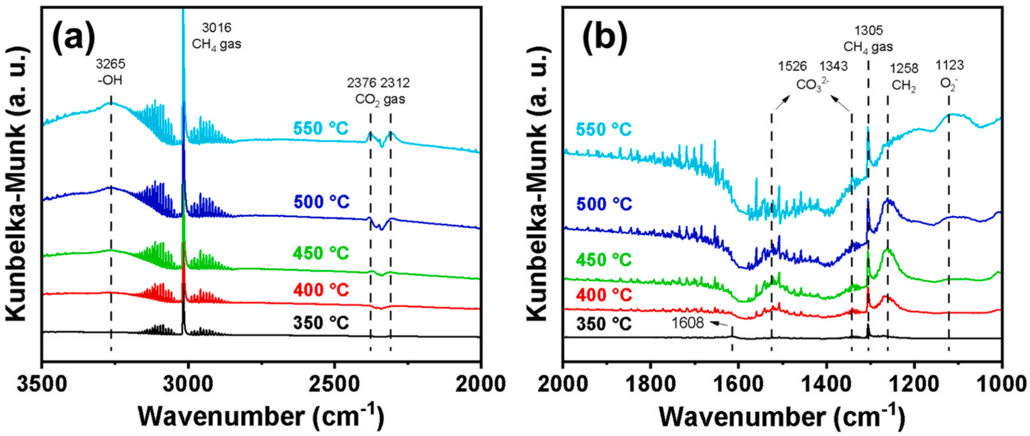

Fig. 5. DRIFTS spectra of CH_4 activation over LFO-H1 at temperatures from 350 °C to 550 °C: (a) in the range of 3500–2000 cm^{-1}, (b) in the range of 2000–1000 cm^{-1}.

gaseous CH_4, which is also reflected by the CH_4 gas band at 3016 cm^{-1}. In the range of 1600–1100 cm^{-1}, several weak bands can be observed, indicating the presence of intermediate species. The bands at 1526 and 1343 cm^{-1} are both ascribed to the bidentate carbonate on the catalyst surface [37,40,41], while the bands at 1258 and 1123 cm^{-1} are ascribed to the δ CH_2 mode alkyl groups bound to metal atoms [42], and absorbed O_2^- [43,44], respectively. The intensity of the band at 1258 cm^{-1} increases up to 500 °C but decreases as the temperature reaches 550 °C, indicating the disappearance of the methanol intermediates [38]. Besides, a weak band at 1608 cm^{-1} can be observed only at 350 °C, assigned to the ketone carbonyl species, which proves a further evidence for the existence of CO_3^{2-} intermediates during CH_4 combustion reaction [45]. These results suggest that the catalysis of CH_4 combustion reaction via acid treated $LaFeO_3$ catalyst is an intricate and multiple process, mainly involving the CH_4 dehydrogenation and the formation of carbonate intermediates.

The acid treatment has led to an increased presence of Fe-O terminations on the surface of LFO-H1, thereby providing more active sites for CH_4 adsorption. On the basis of the above results, we tentatively propose a reaction mechanism for CH_4 combustion on the LFO-H1 surface, as demonstrated in Fig. 6. (1) CH_4 is adsorbed simultaneously at both Fe^{n+} active sites and a nearby lattice oxygen (O_{latt}) [23]. (2) Subsequently, the CH_4 dehydrogenation takes place on the surface of catalyst, where CH_4 is transferred into CH_3* and H* with a homolytic bond breakage. Meanwhile, H* forms an O-H bond with O_{latt}, which initially adsorbs CH_4 in the first step. (3) The dehydrogenation of CH_3* occurs sequentially, forming CH_2*. Simultaneously, H* adsorbs by a neighboring O_{latt}, and one H_2O molecule is generated. (4) CH_2* undergoes homolytic bond breakage into CH* and H*, also forming an O-H bond with O_{latt}. (5) Following the breaking of C-H bond, CH* forms a carbonate intermediate (CO_3^{2-}) through the reaction with two O_{latt} and an oxygen molecule, meanwhile, another H_2O molecule is generated. (6) The carbonate (CO_3^{2-}) is transformed into CO_2 which desorbs at this stage. (7) Finally, molecular O_2 gradually replenishes depleted O_{latt} site to compete a catalytic cycle.

To further investigate the thermal stability and resistance to water of catalyst, a long-term reaction was performed on LFO-H1 at 600 °C. After 18 h continuous heating, a 3 % water dosing was introduced into gas stream. The concentration of CH_4, CO_2 and H_2O were measured, and the results are shown in the Fig. 7. During the initial 18 h, the CH_4 concentration remained relatively stable. Using 1 % as the initial addition, the conversion of CH_4 in the dry condition reached nearly 85 % at 600 °C. Upon introducing water into gas stream, the concentration of CH_4 increased by 0.2 %, indicating the decrease in the catalytic activity due to the presence of water. The reason is attributed to the adsorption of water on the active sites, limiting the adsorption and activation of both oxygen and CH_4 [46]. After discontinuing the water dosing, the concentration of CH_4 returned to the previous level, demonstrating good catalyst recovery. Notably, the CO_2 concentration slightly decreased while the H_2O concentration significantly increased. This observation may be attributed to the reaction mechanism of catalytical CH_4 combustion. As shown in the DRIFTS results, various intermediates can be observed. The decrease in CO_2 concentration may be due to the production of carbon-containing intermediates, disrupting the catalytic reaction cycle required for CO_2 release. The substantial increase in H_2O concentration may be due to the gradual desorption of water molecules, which initially adsorbed on the catalyst surface. Further investigations are needed to gain a comprehensive understanding of the detailed catalytic mechanism in the presence of H_2O, which is the focus of our future research.

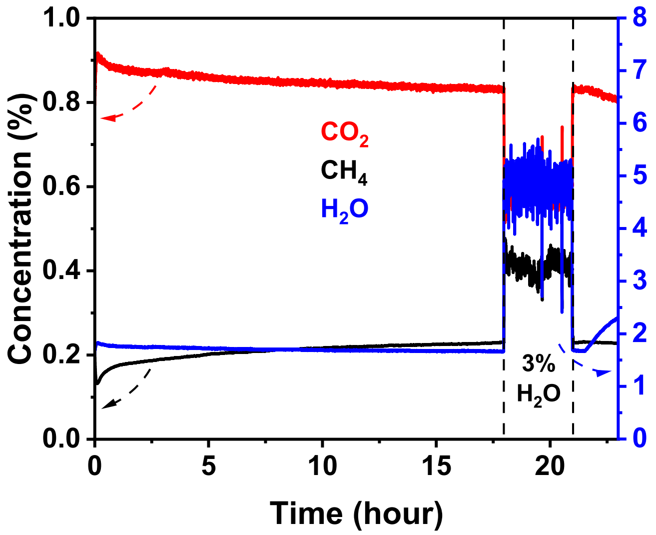

Fig. 7. The concentration of CH_4, CO_2 and H_2O during long-term reaction of LFO-H1.

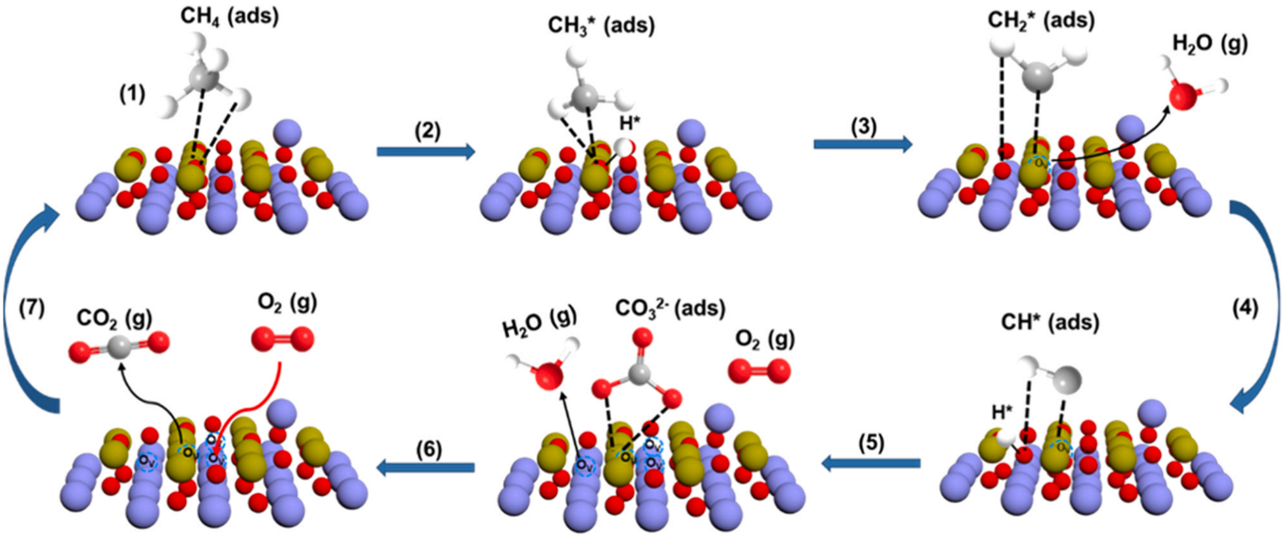

Fig. 6. Scheme of the proposed catalytic reaction mechanism of LFO-H1.

XPS measurement was employed to investigate the surface chemical status of the LFO-H1 catalyst after long-term reaction. As shown in the Figure S9 and Table S3, both Fe^{4+} and Fe^{3+} contents on the surface of the used LFO-H1 catalyst decreased compared to its fresh state. The result aligns with the slight decline in catalytic activity after long-term reaction. High valence state Fe in LFO-H1 facilitates the activation of surface oxygen species, boosting the oxygen absorption and migration kinetics, consequently promoting the methane combustion. During the reaction, oxygen was extracted from the perovskite lattice, leading to the formation of oxygen vacancies and concurrent partial reduction of Fe from Fe^{4+}/Fe^{3+} to lower valence state [47]. Hence, there is a reduction in the Fe^{4+}/Fe^{3+} content in the used catalyst.

4. Conclusion

$LaFeO_3$ perovskite material was synthesized by a sol-gel method, and a subsequent acid etching treatment was performed with different time for the surface modification. The characterization results indicate that the nitric acid preferentially dissolved La cations from $LaFeO_3$ surface, thus more Fe-O termination exposed on the surface of catalyst. Through the evaluation of CH_4 combustion reaction, it is found the appropriate surface acid treatment with 1 h has a discernible impact on the intrinsic reactivity. Among LFO-H1 shows the lowest CH_4 conversion temperature and a good thermal stability, which mainly due to the most Fe active sites on the surface and the lowest energic barriers of CH_4 activation. This work presents a straightforward and effective approach to tailor the exposed surface properties of perovskites, thereby enhancing their activity in hydrocarbon combustion reactions.

CRediT authorship contribution statement

Xiaochao Wu: Writing – review & editing, Supervision, Investigation, Conceptualization. **Ahed Abouserie:** Methodology. **Mengyang Li:** Writing – original draft, Methodology, Investigation. **Gianluca Dalfollo:** Methodology. **Anne Frommelius:** Methodology. **Thorsten Ohlerth:** Methodology. **Ulrich Simon:** Writing – review & editing, Supervision, Resources, Funding acquisition, Conceptualization.

Declaration of Competing Interest

The authors declare that they have no known competing financial interests or personal relationships that could have appeared to influence the work reported in this paper.

Data availability

Data will be made available on request.

Acknowledgments

This work was funded by the Deutsche Forschungsgemeinschaft (DFG, German Research Foundation) under Germany's Excellence Strategy—Cluster of Excellence 2186 "The Fuel Science Center" ID: 390919832. We are grateful to Lena Patterer and Peter Pöllmann, Materials Chemistry, RWTH Aachen University, for their assistance in XPS measurements.

Appendix A. Supporting information

Supplementary data associated with this article can be found in the online version at doi:10.1016/j.cattod.2024.114620.

References

[1] T. Li, Y. Yao, Z. Huang, P. Xie, Z. Liu, M. Yang, J. Gao, K. Zeng, A.H. Brozena, G. Pastel, Denary oxide nanoparticles as highly stable catalysts for methane combustion, Nat. Catal. 4 (2021) 62–70.

[2] Q. Li, X. Chu, Y. Wang, Q. Yang, Z. Su, Y. Peng, W. Si, J. Li, Metal–support interactions within a dual-site Pd/YMn_2O_5 Catalyst during CH_4 combustion, ACS Catal. 12 (2022) 4430–4439.

[3] M. Grubb, C. Vrolijk, D. Brack, Routledge revivals: Kyoto Protocol (1999): A guide and assessment, Routledge2018.

[4] L. He, Y. Fan, J. Bellettre, J. Yue, L. Luo, A review on catalytic methane combustion at low temperatures: catalysts, mechanisms, reaction conditions and reactor designs, Renew. Sustain. Energy Rev. 119 (2020) 109589.

[5] C. Huang, W. Shan, Z. Lian, Y. Zhang, H. He, Recent advances in three-way catalysts of natural gas vehicles, Catal. Sci. Technol. 10 (2020) 6407–6419.

[6] U. Mondal, G.D. Yadav, Methanol economy and net zero emissions: critical analysis of catalytic processes, reactors and technologies, Green Chem. 23 (2021) 8361–8405.

[7] Y. Feng, Y. Liu, H. Dai, J. Deng, Review and perspectives of enhancement in the catalytic stability for the complete combustion of CO, CH_4, and volatile organic compounds, Energy Fuels 37 (2023) 3590–3604.

[8] J. Yang, M. Peng, G. Ren, H. Qi, X. Zhou, J. Xu, F. Deng, Z. Chen, J. Zhang, K. Liu, A Hydrothermally stable irreducible oxide-modified $Pd/MgAl_2O_4$ catalyst for methane combustion, Angew. Chem. 132 (2020) 18680–18684.

[9] S. Yasumura, K. Saita, T. Miyakage, K. Nagai, K. Kon, T. Toyao, Z. Maeno, T. Taketsugu, K.-I. Shimizu, Designing main-group catalysts for low-temperature methane combustion by ozone, Nat. Commun. 14 (2023) 3926.

[10] F. Polo-Garzon, V. Fung, J. Zhang, Z. Bao, H.M. Meyer III, M. Kidder, Z. Wu, CH_4 Activation over perovskite catalysts: true density and reactivity of active sites, ACS Catal. 12 (2022) 11845–11853.

[11] X. Yuan, L. Meng, C. Zheng, H. Zhao, Deep Insight into the Mechanism of Catalytic Combustion of CO and CH_4 over $SrTi_{1-x}B_xO_3$ (B= Co, Fe, Mn, Ni, and Cu) Perovskite via Flame Spray Pyrolysis, ACS Appl. Mater. Interfaces 13 (2021) 52571–52587.

[12] S.D. Mürtz, J. Simböck, F. Zeng, M. Ghiasi, S. Schönebaum, U. Simon, F.M. de Groot, R. Palkovits, Elucidating the validity of electronic characteristics of transition metal perovskites as descriptors bridging electro-and chemocatalysis, EES Catal. 1 (2023) 961–971.

[13] X. Wu, M. Fischer, A. Nolte, P. Lenßen, B. Wang, T. Ohlerth, D. Wöll, K.A. Heufer, S. Pischinger, U. Simon, Perovskite catalyst for in-cylinder coating to reduce raw pollutant emissions of internal combustion engines, ACS Omega 7 (2022) 5340–5349.

[14] F. Fang, N. Feng, L. Wang, J. Meng, G. Liu, P. Zhao, P. Gao, J. Ding, H. Wan, G. Guan, Fabrication of perovskite-type macro/mesoporous $La_{1-x}K_xFeO_{3-\delta}$ nanotubes as an efficient catalyst for soot combustion, Appl. Catal. B 236 (2018) 184–194.

[15] D. Yang, M. Cao, Q. Zhong, P. Li, X. Zhang, Q. Zhang, All-inorganic cesium lead halide perovskite nanocrystals: synthesis, surface engineering and applications, J. Mater. Chem. C 7 (2019) 757–789.

[16] Y. Tang, C.H. Mak, G. Jia, K.-C. Cheng, J.-J. Kai, C.-W. Hsieh, F. Meng, W. Niu, F.-F. Li, H.-H. Shen, Lead-free hybrid perovskite photocatalysts: surface engineering, charge-carrier behaviors, and solar-driven applications, J. Mater. Chem. A 10 (2022) 12296–12316.

[17] C. Xie, Z. Niu, D. Kim, M. Li, P. Yang, Surface and interface control in nanoparticle catalysis, Chem. Rev. 120 (2019) 1184–1249.

[18] W. Qin, R. Zhang, Z. Yuan, Y. Shen, G. Wang, F. Meng, Exposure surface active sites of perovskite-type $LaFeO_3$ gas sensors by selectively dissolving la cations for enhancing gas sensing properties to acetone, Adv. Mater. Technol. 7 (2022) 2200255.

[19] C. Aranthady, T. Jangid, K. Gupta, A.K. Mishra, S. Kaushik, V. Siruguri, G.M. Rao, G.V. Shanbhag, N.G. Sundaram, Selective SO_2 detection at low concentration by Ca substituted $LaFeO_3$ chemiresistive gas sensor: a comparative study of $LaFeO_3$ pellet vs thin film, Sens. Actuators B 329 (2021) 129211.

[20] D. Neagu, G. Tsekouras, D.N. Miller, H. Ménard, J.T. Irvine, In situ growth of nanoparticles through control of non-stoichiometry, Nat. Chem. 5 (2013) 916–923.

[21] W. Si, Y. Wang, Y. Peng, J. Li, Selective dissolution of A-site cations in ABO_3 perovskites: a new path to high-performance catalysts, Angew. Chem. 127 (2015) 8065–8068.

[22] K. Huang, X. Chu, L. Yuan, W. Feng, X. Wu, X. Wang, S. Feng, Engineering the surface of perovskite $La_{0.5}Sr_{0.5}MnO_3$ for catalytic activity of CO oxidation, Chem. Commun. 50 (2014) 9200–9203.

[23] J. Yang, S. Hu, L. Shi, S. Hoang, W. Yang, Y. Fang, Z. Liang, C. Pan, Y. Zhu, L. Li, Oxygen vacancies and lewis acid sites synergistically promoted catalytic methane combustion over perovskite oxides, Environ. Sci. Technol. 55 (2021) 9243–9254.

[24] Q. Yang, J. Li, D. Wang, Y. Peng, Y. Ma, Activity improvement of acid treatment on $LaFeO_3$ catalyst for CO oxidation, Catal. Today 376 (2021) 205–210.

[25] P. Coutinho, F. Cunha, P. Barrozo, Structural, vibrational and magnetic properties of the orthoferrites $LaFeO_3$ and $YFeO_3$: a comparative study, Solid State Commun. 252 (2017) 59–63.

[26] W. Guo, L. Cui, H. Xu, C. Gong, Selective dissolution of A-site cations of $La_{0.6}Sr_{0.4}Co_{0.8}Fe_{0.2}O_3$ perovskite catalysts to enhance the oxygen evolution reaction, Appl. Surf. Sci. 529 (2020) 147165.

[27] Q. Yang, D. Wang, C. Wang, X. Li, K. Li, Y. Peng, J. Li, Facile surface improvement method for $LaCoO_3$ for toluene oxidation, Catal. Sci. Technol. 8 (2018) 3166–3173.

[28] P. Garcia-Muñoz, F. Fresno, C. Lefevre, D. Robert, N. Keller, Synergy effect between photocatalysis and heterogeneous photo-Fenton catalysis on Ti-doped $LaFeO_3$ perovskite for high efficiency light-assisted water treatment, Catal. Sci. Technol. 10 (2020) 1299–1310.

[29] X. Wang, J. Dai, C. Zhou, D. Guan, X. Wu, W. Zhou, Z. Shao, Engineering charge redistribution within perovskite oxides for synergistically enhanced overall water splitting, ACS Mater. Lett. 3 (2021) 1258–1265.

[30] V. Bashan, Y. Ust, Perovskite catalysts for methane combustion: applications, design, effects for reactivity and partial oxidation, Int. J. Energy Res. 43 (2019) 7755–7789.

[31] W. Xia, K. Leng, Q. Tang, L. Yang, Y. Xie, Z. Wu, K. Yi, X. Zhu, Structural characterization, magnetic and optical properties of perovskite $(La_{1-x}Ln_x)_{0.67}Ca_{0.33}MnO_3$ (Ln= Nd and Sm; x= 0.0–0.5) nanoparticles synthesized via the sol-gel process, J. Alloy. Compd. 867 (2021) 158808.

[32] B. Kucharczyk, J. Okal, W. Tylus, J. Winiarski, B. Szczygieł, The effect of the calcination temperature of $LaFeO_3$ precursors on the properties and catalytic activity of perovskite in methane oxidation, Ceram. Int. 45 (2019) 2779–2788.

[33] M. Wu, S. Chen, W. Xiang, Oxygen vacancy induced performance enhancement of toluene catalytic oxidation using $LaFeO_3$ perovskite oxides, Chem. Eng. J. 387 (2020) 124101.

[34] L. Ren, Z. Huo, S. Song, H. Yu, B. Tan, Y. Wang, N. Feng, H. Wan, G. Guan, Surface tuning of 3DOM $LaFe_{0.6}Mg_{0.4}O_3$ perovskite by acid etching to enhance catalytic performance for soot combustion, Appl. Surf. Sci. 629 (2023) 157435.

[35] A.A. Ansari, N. Ahmad, M. Alam, S.F. Adil, M.E. Assal, A. Albadri, A.M. Al-Enizi, M. Khan, Optimization of Redox and Catalytic Performance of $LaFeO_3$ Perovskites: Synthesis and Physicochemical Properties, J. Electron. Mater. 48 (2019) 4351–4361.

[36] G. Li, C. Zhang, Z. Wang, H. Huang, H. Peng, X. Li, Fabrication of mesoporous Co_3O_4 oxides by acid treatment and their catalytic performances for toluene oxidation, Appl. Catal. A 550 (2018) 67–76.

[37] P.J. Jodłowski, R.J. Jędrzejczyk, D. Chlebda, M. Gierada, J. Łojewska, In situ spectroscopic studies of methane catalytic combustion over Co, Ce, and Pd mixed oxides deposited on a steel surface, J. Catal. 350 (2017) 1–12.

[38] X. Cao, R. Zhou, N. Rui, Z. Wang, J. Wang, X. Zhou, C.-J. Liu, Co_3O_4/HZSM-5 catalysts for methane combustion: The effect of preparation methodologies, Catal. Today 297 (2017) 219–227.

[39] H. Chen, S. Chansai, S. Xu, S. Xu, Y. Mu, C. Hardacre, X. Fan, Dry reforming of methane on bimetallic Pt–Ni@CeO_2 catalyst: a in situ DRIFTS-MS mechanistic study, Catal. Sci. Technol. 11 (2021) 5260–5272.

[40] T. Li, M. Dong, J. Xu, T. Zhang, Y. Sun, N. Li, Z. Wu, J. Li, E. Gao, J. Zhu, Exploring the promotion of γ-Al_2O_3 on Pd/CeO_2-catalyzed low-concentration methane oxidation using operando DRIFTS-MS, ChemCatChem 15 (2023) e202300194.

[41] M. Gao, Z. Gong, X. Weng, W. Shang, Y. Chai, W. Dai, G. Wu, N. Guan, L. Li, Methane combustion over palladium catalyst within the confined space of MFI zeolite, Chin. J. Catal. 42 (2021) 1689–1699.

[42] I. Kretzschmar, J.A. Levinson, C.M. Friend, Hydroxymethylcyclopropane on oxygen-covered Mo (110): A radical clock on a surface, J. Am. Chem. Soc. 122 (2000) 12395–12396.

[43] J. Li, X. Liang, S. Xu, J. Hao, Catalytic performance of manganese cobalt oxides on methane combustion at low temperature, Appl. Catal. B 90 (2009) 307–312.

[44] K. Li, K. Liu, D. Xu, H. Ni, F. Shen, T. Chen, B. Guan, R. Zhan, Z. Huang, H. Lin, Lean methane oxidation over $Co_3O_4/Ce_{0.75}Zr_{0.25}$ catalysts at low-temperature: Synergetic effect of catalysis and electric field, Chem. Eng. J. 369 (2019) 660–671.

[45] Q. Li, Y. Wang, W. Si, Y. Peng, J. Li, Novel Insights on the Metal–Support Interactions of Pd/ZrO_2 Catalysts on CH_4 Oxidation, ACS Appl. Mater. Interfaces 15 (2023) 7959–7968.

[46] W. Huang, X. Zhang, A.-C. Yang, E.D. Goodman, K.-C. Kao, M. Cargnello, Enhanced catalytic activity for methane combustion through in situ water sorption, ACS Catal. 10 (2020) 8157–8167.

[47] S. Das, S. Bhattar, L. Liu, Z. Wang, S. Xi, J.J. Spivey, S. Kawi, Effect of partial Fe substitution in $La_{0.9}Sr_{0.1}NiO_3$ perovskite-derived catalysts on the reaction mechanism of methane dry reforming, ACS Catal. 10 (2020) 12466–12486.